Volume 13 | Number 4 | 28 January 2015 | Pages 957–1266

Organic & Biomolecular Chemistry

www.rsc.org/obc

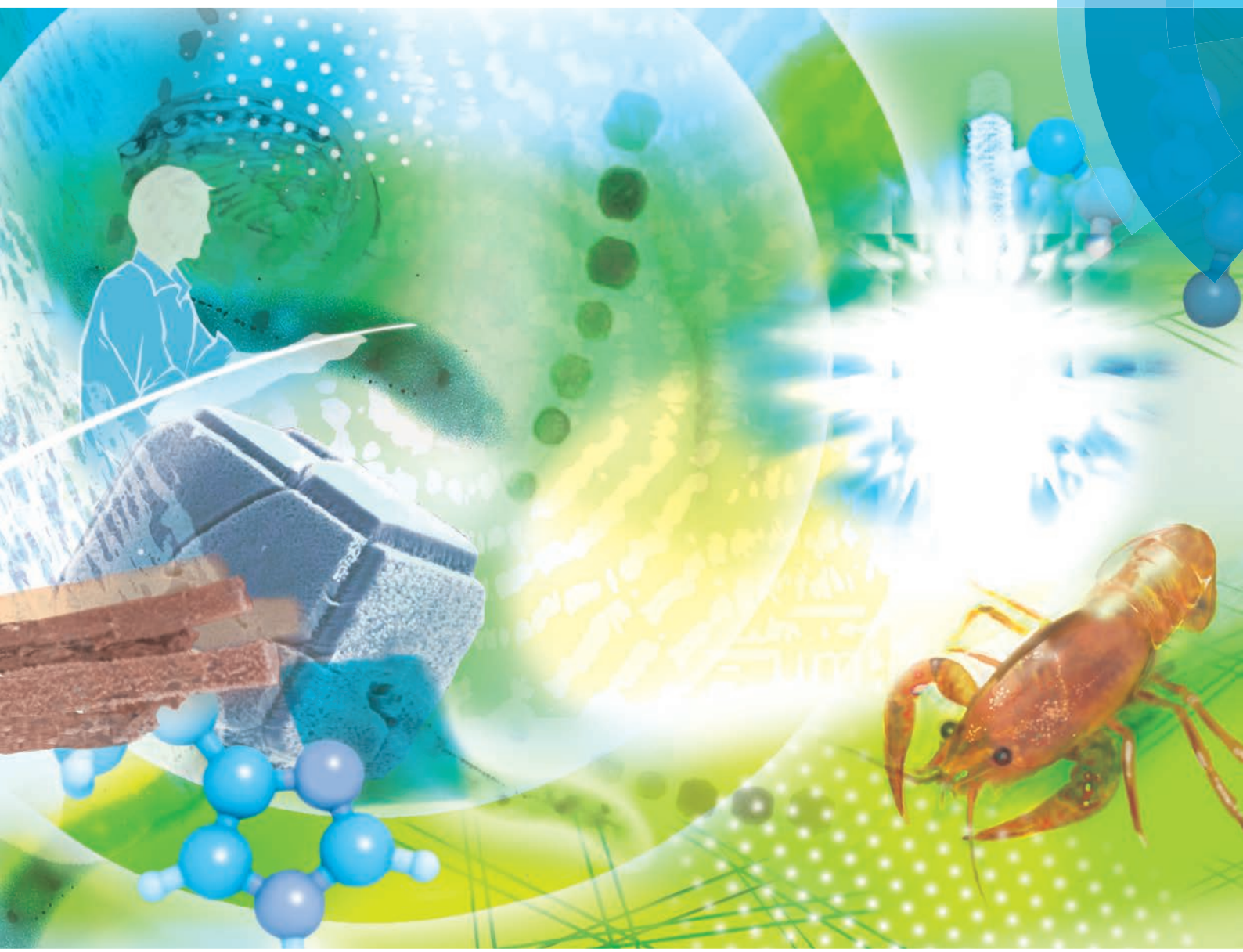

ISSN 1477-0520

ROYAL SOCIETY OF CHEMISTRY

REVIEW ARTICLE
Atsushi Arakaki, Takashi Kato *et al.*
Biomineralization-inspired synthesis of functional organic/inorganic hybrid materials: organic molecular control of self-organization of hybrids

Organic & Biomolecular Chemistry

REVIEW

View Article Online
View Journal | View Issue

Cite this: *Org. Biomol. Chem.*, 2015, **13**, 974

Biomineralization-inspired synthesis of functional organic/inorganic hybrid materials: organic molecular control of self-organization of hybrids

Atsushi Arakaki,*[a] Katsuhiko Shimizu,[b] Mayumi Oda,[a] Takeshi Sakamoto,[c] Tatsuya Nishimura[c] and Takashi Kato*[c]

Organisms produce various organic/inorganic hybrid materials, which are called biominerals. They form through the self-organization of organic molecules and inorganic elements under ambient conditions. Biominerals often have highly organized and hierarchical structures from nanometer to macroscopic length scales, resulting in their remarkable physical and chemical properties that cannot be obtained by simple accumulation of their organic and inorganic constituents. These observations motivate us to create novel functional materials exhibiting properties superior to conventional materials—both synthetic and natural. Herein, we introduce recent progress in understanding biomineralization processes at the molecular level and the development of organic/inorganic hybrid materials by these processes. We specifically outline fundamental molecular studies on silica, iron oxide, and calcium carbonate biomineralization and describe material synthesis based on these mechanisms. These approaches allow us to design a variety of advanced hybrid materials with desired morphologies, sizes, compositions, and structures through environmentally friendly synthetic routes using functions of organic molecules.

Received 22nd August 2014,
Accepted 14th October 2014

DOI: 10.1039/c4ob01796j

www.rsc.org/obc

Introduction

Biominerals are organic/inorganic hybrid materials that are essential components of living organisms and support important functions. Typical examples are hydroxyapatite ($Ca_{10}(PO_4)_6(OH)_2$) in bones and teeth of mammals,[1] calcium carbonate ($CaCO_3$) in molluscan shells,[2] amorphous silica (SiO_2) in diatoms[3] and marine sponges,[4] and magnetite (Fe_3O_4) in chiton teeth.[5] These biominerals have elaborate hierarchical structures giving them conspicuously high mechanical hardness and flexibility, which are not provided by conventional synthetic materials.[6,7] Single calcite crystals found in the skeletal construction of brittle stars are a component of specialized photosensory organs, possibly functioning as a compound eye.[8] Magnetite nanocrystals in some organisms such as birds and bacteria function as biological geomagnetic sensors that help them find and survive in their habitats on the earth.[9] The optical and mechanical properties of biominerals are derived from their complex structures consisting of organic and inorganic constituents.[7,10,11] Most biominerals are formed using abundant elements in earth's crust. Moreover, they are synthesized under mild conditions at a near-neutral pH and ambient temperature. Owing to these interesting features, the formation processes of biominerals have attracted much attention with the aim of understanding the mechanisms and applying them to material synthesis in industry.

Over the last three decades, a number of proteins that control biomineralization processes, including promotion of crystal formation,[3,4,12] matrix-assisted orientation of crystals,[13,14] growth inhibition by face-selective surface adsorption,[15,16] and control of the crystal phase,[16,17] have been isolated and analyzed (Table 1). Although it has been believed that proteins play important roles in biomineralization processes, most studies are still limited to fundamental analyses of proteins, such as amino acid sequence comparisons and biochemical characterization. The functions of proteins at the molecular level have remained largely unknown so far. A significant breakthrough in material synthesis using a biomineralization protein was achieved by a study involving sponges.[18] The protein—known as silicatein—was isolated from silica spicules that form the skeletal structures of marine sponges.[4] Surprisingly, this protein shows a direct catalytic function of silica biomineralization and it allows us to synthesize new materials

[a]*Division of Biotechnology and Life Science, Institute of Engineering, Tokyo University of Agriculture and Technology, 2-24-16, Naka-cho, Koganei, Tokyo 184-8588, Japan. E-mail: arakakia@cc.tuat.ac.jp*
[b]*Organization for Regional Industrial Academic Cooperation, Tottori University, 4-101, Minami, Koyama-cho, Tottori 680-8550, Japan*
[c]*Department of Chemistry and Biotechnology, School of Engineering, The University of Tokyo, Hongo, Bunkyo-ku, Tokyo 113-8656, Japan. E-mail: kato@chiral.t.u-tokyo.ac.jp*

with a non-natural composition and a wide spectrum of properties.[19,20] After the identification of silicatein, many proteins were isolated from various biominerals in diverse organisms, which encouraged researchers to use them for material synthesis.[3,14,17] Silaffins isolated from diatoms can induce and regulate silica precipitation.[3] A small iron-binding protein, Mms6, isolated from magnetotactic bacteria regulates the surface structure of magnetite nanoparticles.[17] A calcium-binding protein, Pif, regulates the nacre formation in the pearl oyster *Pinctada fucata*.[14] These proteins, isolated from different biominerals, opened the door for bio-inspired synthesis of functional organic/inorganic hybrid materials with controlled micro- to nanoscale properties. On the basis of these fundamental molecular studies, the functional regions of organic molecules have been adopted for biomimetic nanofabrication processes and the development of bio-inspired materials.[21–25]

In this review, we introduce the recent advances in the fundamental molecular analyses of biomineralization in several biological systems. Here, we focus on the studies on silica, iron oxide, and calcium carbonate (Fig. 1). We also emphasize the application of the proteins associated with biomineralization toward the controlled synthesis of organic/inorganic functional materials.

Table 1 Examples of proteins directly involved in calcium carbonate, silica, and iron oxide biomineralization

Protein	Biomineral	Function	References
Calcium carbonate			
Perlucin	The nacreous layer of the shell	Calcite precipitation	12
MSI31, 60	The nacreous layer of the shell	Framework of the prismatic layer	13
Pif	The nacreous layer of the shell	Aragonite crystal formation	14
Ansocalcin	Goose egg shell matrix	Template for calcite nucleation	15
CAP-1	The exoskeleton of crayfish	Crystal growth regulation	16
Silica			
Silicatein	Sponge spicules	Silica polymerization	4
Silaffin	Diatom shells	Silica precipitation	3
Iron oxide			
Mms6	Bacterial magnetites	Crystal size and shape control of magnetites	17

Silica biomineralization and application

Learning the essence of silica biomineralization in sponges

Silicon (Si) is the second most abundant element in the earth's crust, existing naturally as silicon dioxide or silicates. This common element is incorporated into a wide range of living organisms, including diatoms, sponges, and higher plants, which produce structures composed of amorphous hydrated silica.[26] Biological siliceous structures (biosilica) are synthesized by biological processes and possess exquisite species-specific morphology with sizes ranging from the nanometer to, occasionally, the meter scale.[26] Organic molecules, whose expression is under the control of genetic information, determine the uniqueness of biosilica. Scientists have taken advantage of recent advances in molecular biology and analytical technology to explore the organic molecules involved in biosilicification.[3,4,27–29] Understanding its mechanism will lead to the development of new routes to synthesize functional materials under environmentally benign conditions.

Biosilica occurs in sponges in the form of structures called spicules that are needle shaped, with dimensions ranging

Atsushi Arakaki

Atsushi Arakaki received his PhD from the Tokyo University of Agriculture and Technology in 2003 under the supervision of Prof. Tadashi Matsunaga. After his postdoctoral research at Waseda University, Japan, he joined the Tokyo University of Agriculture and Technology and became an associate professor in 2011. His current research focuses on understanding the mechanism controlling the magnetite morphology in magnetotactic bacteria and utilization of this mechanism for developing functional magnetic materials. He is a principal investigator of the "Fusion Materials" project.

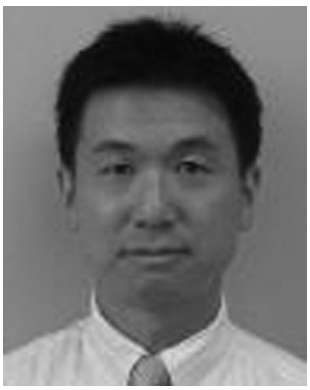

Katsuhiko Shimizu

Katsuhiko Shimizu received his PhD in Biological Science at Tokyo Metropolitan University in 1992. He conducted his postdoctoral research at several institutions, including the Fusetani Biofouling Project, Exploratory Research for Advanced Technology (ERATO), Research Development Corporation of Japan (JRDC), and the University of California Santa Barbara under the guidance of Prof. Daniel E. Morse. He joined Tottori University, Japan, as an associate professor in 2010. His current research focuses on understanding the molecular mechanisms controlling silicon biomineralization in sponges for the development of novel, environmentally benign routes for manufacturing silicon-based inorganic–organic composite materials. He is a principal investigator of the "Fusion Materials" project.

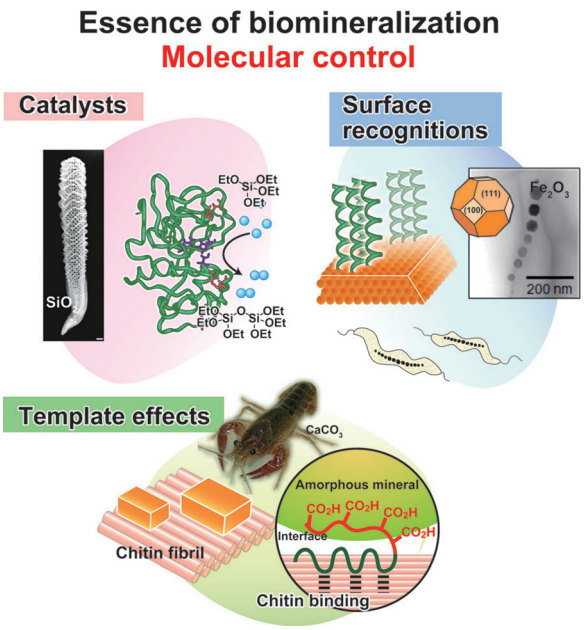

Fig. 1 Schematic illustration of molecularly controlled processes of biomineralization.

from micrometer to millimeter scales. However, some exceptions also exist; *e.g.*, in the case of the hexactinellid sponge *Monorhaphis chuni*, the basal spicules can be as long as 3 m (diameter, 1 cm) and are the largest known biosilica structures on the earth (Fig. 2).[30,31] Spicules of the Venus' flower basket sponge *Euplectella aspergillum* are exquisitely weaved to construct skeletons that

Takashi Kato

Takashi Kato received his PhD from the University of Tokyo in 1988. After doing postdoctoral research at Cornell University under the guidance of Prof. Jean M. J. Fréchet, he joined the University of Tokyo where he is currently a professor. His research highlights the development of self-assembled materials, including supramolecular materials, liquid crystals, gels, ion-, electro-, and photo-functional materials, functional polymers, and bio-inspired organic/inorganic hybrids. He has published about 400 papers including original manuscripts, reviews, and chapters of books. He is an editorial and advisory board member of several scientific journals including RSC journals: Chem. Sci., J. Mater. Chem. C and New J. Chem. He is the project leader of a project of Grant-in-Aid for Scientific Research (KAKENHI) on Innovative Areas funded by the Ministry of Education, Culture, Sports, Science and Technology, Japan (MEXT): "Fusion Materials: Creative Development of Materials and Exploration of Their Function through Molecular Control".

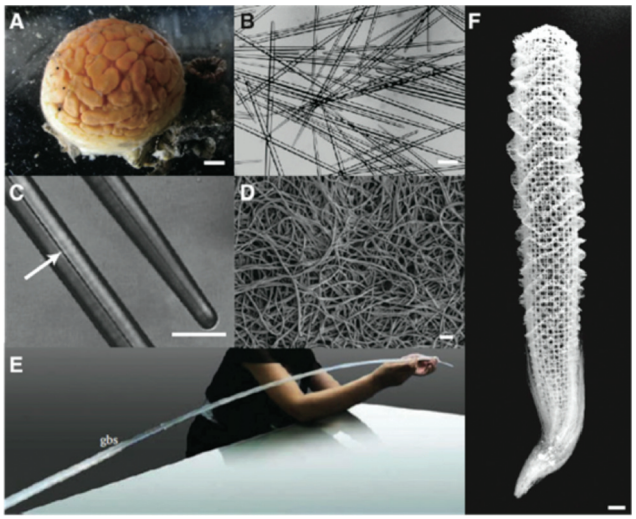

Fig. 2 Sponge biosilica. (A) Demosponge *Tethya aurantia*. (B) Spicules of *T. aurantia*. (C) Enlarged image of (B) with an arrow indicating an axial filament that is composed of silicateins. (D) Axial filaments isolated by dissolving silica spicules. (B–D) Reproduced with permission from ref. 30. Copyright Wiley 2003 Wiley Periodicals Inc. (E) Giant basal spicules (gbs) from *Monorhaphis chuni*, with a length of 270 cm and a diameter of 10 mm. Reproduced from ref. 31. (F) Silica skeleton of the Venus flower basket sponge *Euplectella aspergillum*.

are hierarchically arranged with nano- to meter-scale structures. In sponges, the biosilica shows remarkable mechanical toughness and optical properties[10] and provides support for the body, protection against predators, and light guides.

Each silica spicule contains a proteinous central core along the long axis, called the axial filament.[4] The protein filaments were isolated from the demosponge *Tethya aurantia* by dissolving the surrounding silica with HF and dissociated to yield three similar proteins: silicatein α, β, and γ (Table 1).[4] Their molecular weights (27–29 kDa) and amino acid compositions are similar, suggesting that they are members of a single protein family. The amino acid sequence of silicatein α reveals that the protein is similar to cathepsin L and members of the papain-like cysteine protease family. The cysteine protease is named after the cysteine (Cys) at the active site; however, the amino acid at the corresponding site in silicateins is occupied by serine (Ser) (Fig. 3A). The Cys residues that form intramolecular disulfide bridges in the proteases are conserved, suggesting that the tertiary conformations of these proteins are also similar.[18]

Since the first identification in *T. aurantia*, silicateins have been isolated from a wide variety of demosponge species.[32–35] The demosponges *Geodia cydonium* and *Ephydatia fluviatilis* possess two morphologically different spicules.[34,35] The characteristic morphology of spicules is considered to be due to the specific properties and combinatory functions of silicatein isoforms. Silicatein has also been identified in the hexactinellid sponges, *Monorhaphis chuni*,[36] *Crateromorpha meyeri*,[37] and *Aulosaccus schulzei*, suggesting that silicatein is a common protein in sponges.[38]

Silicateins probably play two roles in sponge spicule formation. First, a catalytic role in sponge silica biomineralization

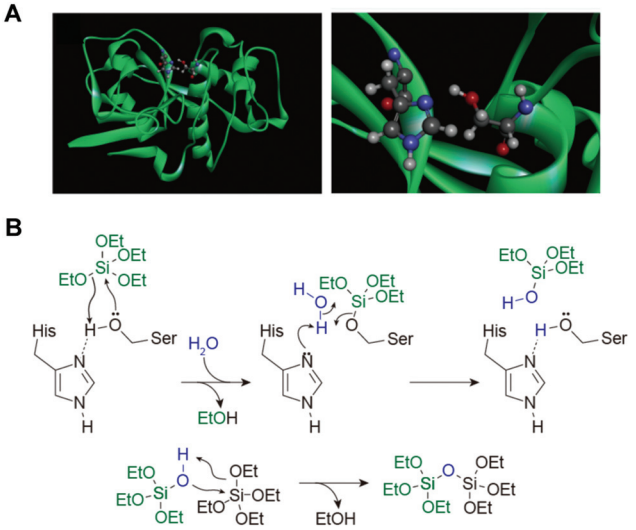

Fig. 3 (A) Ribbon model of silicatein α (in green) (left) and enlarged serine-hydrolase catalytic site (right). At the site, a nucleophilic serine residue is presented for hydrogen-bonding with imidazole that enhances the hydrolytic activity of the enzyme.[20] (B) Proposed reaction mechanism of hydrolysis of tetraethoxysilane and polycondensation of silica, as catalyzed by silicatein α. Proposed mechanism is based on a well-characterized mechanism of catalytic hydrolysis of peptide bonds by serine proteases.[18]

is suggested. Cha *et al.*[18] demonstrated that the axial filaments isolated from *T. aurantia* catalyzed the hydrolysis of various silicon alkoxides such as tetraethoxysilane (TEOS) and methyl- and phenyl-triethoxysilanes to yield silica and the corresponding silsesquioxanes *in vitro* at ambient temperature, pressure, and neutral pH. This activity was retained in silicatein monomers dissociated from the axial filaments and also reproduced with a recombinant form synthesized in genetically engineered *Escherichia coli*.[39] The mutant silicateins, constructed by replacing the putative active site Ser (with a hydroxyl side-chain) at position 26 and/or His (with an imidizole side-chain) at position 165 of silcatein α with alanine (with a methyl side-chain), significantly decreased silica formation from the alkoxide substrate.[39] Based on the mechanism for catalytic hydrolysis of the peptide bonds by the serine proteases (*e.g.*, chymotrypsin, trypsin), in conjunction with the results of the site-directed mutagenesis experiments, the hydrolysis of silicon alkoxides and polymerization of silicic acids by silicatein are explained as follows (Fig. 3B).[18] The Ser 26–His 165 side-chain couple in silcatein α to hydrolyze the silicon alkoxides acts as the active-site Ser–His pair for the serine proteases to catalyze peptide bond hydrolysis.[20]

The second role of silicateins is the templating and construction of the axial filaments within the structure. Self-assembly of the silicatein to form a filamentous structure appears to be mediated by the interaction of hydrophobic patches on the surfaces of the silicatein isoforms.[40] The filaments guide the deposition of the polycondensed silica product along the entire filament length.[18] This activity is abolished by treatment with heat or a detergent (sodium dodecylsulfate).[18]

Application of silicateins and sponge-biosilicification

Since the dual functions of silicatein were characterized, it has been widely used directly, as well as in a biologically motivated manner, for the synthesis of silica and other industrially important inorganic materials under mild conditions.[41–44]

The discovery that silicatein filaments prepared from *T. aurantia* can biocatalytically hydrolyze silicon alkoxides and template the products led us to apply this technology to the synthesis and templating of other metal(loid) oxide materials. For example, nanocrystalline anatase TiO_2 were prepared from titanium(IV) bis(ammonium lactato)dihydroxide (Ti(BALDH)), a water-stable alkoxide-like conjugate of titanium.[45] Oriented aggregates of Ga_2O_3 nanocrystals were obtained from $Ga(NO_3)_3$,[46] and nanostructured $BaTiOF_4$,[19] which is an intermediate for production of $BaTiO_3$, was formed from $BaTiF_6$ under ambient conditions. Silicateins are arranged to form a perfect lattice which templates a 3D mesoporous silica structure in a *Monorhaphis chuni* giant spicule.[47] This capability was used to synthesize cristobalite and remarkable flexible rods of aligned calcite nanocrystals.[48,49]

Production of recombinant silicateins by genetic engineering broadens opportunities for application of these catalysts for manufacturing inorganic materials through environmentally benign routes. Recombinant silicatein catalyzes condensation of alkoxysilanes at neutral pH and ambient temperature to yield silica as well as silicones such as straight-chained poly(dimethylsiloxane) (PDMS).[50] The formation of uniform silica films with controlled thickness, roughness, and hydrophilicity was achieved using immobilized silicateins on gold-coated surfaces, polystyrene, and silicon wafers.[51] Recombinant silicateins were immobilized on silicon substrates by a microcontact printing-based physisorption method. Incubation of the immobilized recombinant silicatein with TEOS produced biosilica microstructures and/or silica films by simply varying the reaction time in precursor solution.[52] Electrical insulation properties were demonstrated for potential device applications. Recombinant silicateins can be modified with the fusion of additional peptide sequences, including polyHis (His-tag), bearing a strong affinity to Ni^{2+} or Co^{2+} chelated with nitrilotriacetic acid (NTA), and polyglutamate (Glu-tag), with the affinity to hydroxyapatite, making them remarkably useful tools for immobilization. Tahir *et al.*[53,54] showed that the recombinant silicatein with His-tag bound to the gold surface with Ni-NTA retained its biocatalytic activity to produce layered arrangements of titania and zirconia from Ti(BALDH) and hexafluorozirconate, respectively, in addition to silica from TEOS. Titania coating from Ti(BALDH) on the surface of the WS2 nanotubes was also mediated by the immobilized silicatein (Fig. 4). To prepare silicatein-immobilized WS_2 nanotubes, the nanotubes were covered with the polymers carrying NTA side-chains, and then a His-tagged silicatein was bound to the surface of the polymer-coated WS_2 nanotubes through NTA.[55] Nanostructured cassiterite SnO_2 was synthesized from sodium hexafluorostannate by the catalytic activity of His-tagged silicatein immobilized on glass surfaces using an NTA anchor.[56]

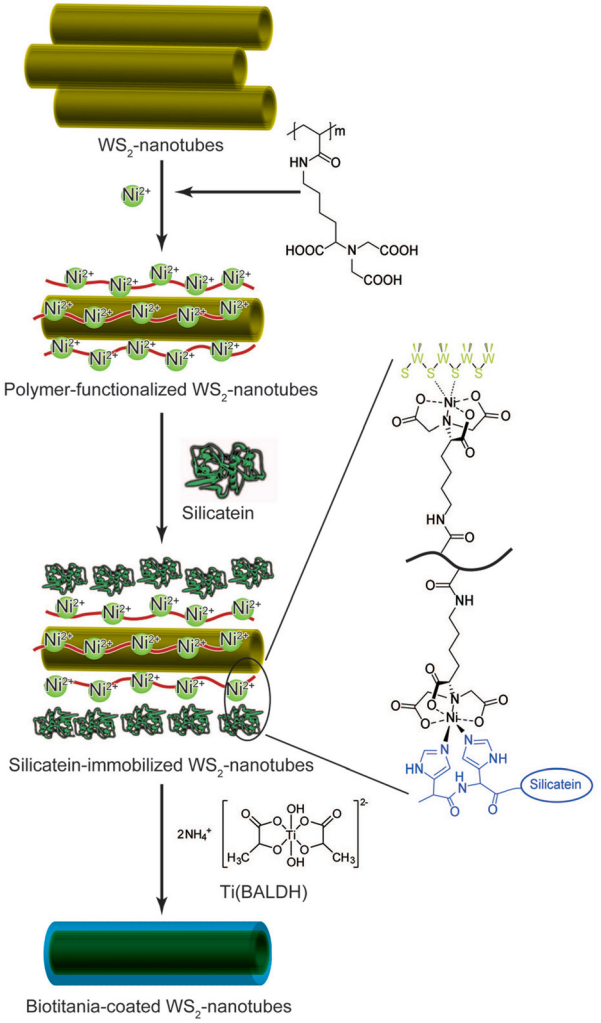

Fig. 4 Schematic illustration for preparation of biotitania-coated inorganic nanotubes using silicatein.[55]

The immobilized His-tagged silicatein on magnetite nanoparticles also retains its native hydrolytic activity to catalyze the formation of silica by copolymerization of TEOS.[57] His-tagged silicatein acts as a nanoreactor to synthesize and immobilize gold nanoparticles obtained from auric acid onto the core–shell polymer colloids, although the mechanism of gold synthesis in the presence of silicatein is not uncovered.[58]

The development and availability of recombinant silicatein opens new possibilities for biomaterial and medical applications. Tissue culture plates modified with silicatein-mediated deposition of silica enhanced the activity of bone-mineralizing cells.[59] Glu-tag-immobilized recombinant silicateins catalyzed the synthesis of biosilica coatings from sodium metasilicate on both synthetic hydroxyapatite nanofibrils and dental hydroxyapatite.[60] This technology indicates that Glu-tagged silicateins have considerable biomedical potential with regenerative and prophylactic implementations.

Based on the essential participation of specific Ser and His residues in silicatein's catalytic active site, a synthetic mimic that provides both catalysis and the surface determinants

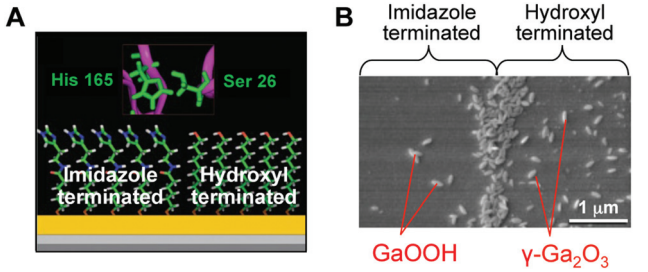

Fig. 5 (A) Schematic representation of self-assembled monolayer domains providing the necessary juxtaposition of hydroxyl and imidazole moieties to catalyze the hydrolysis of the gallium oxide precursor and template the condensed product to form GaOOH and γ-Ga_2O_3. (B) SEM image of GaOOH and γ-Ga_2O_3 formed on a self-assembled monolayer surface. Reproduced with permission from ref. 20. Copyright 2005 National Academy of Sciences.

necessary to structurally direct heterogeneous nucleation by condensation was developed. Kisailus *et al.*[61] prepared gold nanoparticles separately functionalized with hydroxy (nucleophilic) and imidazole (hydrogen bonding) groups. The catalytic activity of silicatein was mimicked by a mixture of two gold nanoparticle types. When the two gold nanoparticles were mixed with TEOS at room temperature and neutral pH, silica production was observed. Subsequently, using lithographically patterned PDMS stamps, bifunctional self-assembled monolayer surfaces were fabricated with hydroxy- and imidazole-functionalized alkane thiols on gold substrates.[20] The interface between chemically distinct self-assembled monolayer domains provided the necessary juxtaposition of nucleophilic (hydroxyl) and hydrogen-bonding (imidazole) agents to catalyze the hydrolysis of a Ga_2O_3 precursor and template the condensed product to form GaOOH and the defect spinel γ-Ga_2O_3 (Fig. 5). Using this approach, the production of patterned substrates for catalytic synthesis and templating of semiconductors for device applications can be envisioned. Silicateins inspired Adamson *et al.*[62] to synthesize a catalytically active block copolymer poly(2-vinylpyridine-*b*-1,2-butadiene) functionalized by the introduction of hydroxyl groups at butadiene, which showed the catalytic action of the polymer on TEOS under neutral pH and ambient temperature conditions. Lee *et al.*[63] demonstrated that the dipeptide His–Ser, mimicking the catalytic structure of silicatein, was used as an additive in the $Ga(NO_3)_3$ solution to form spindle-shaped GaOOH crystals, while only irregularly shaped aggregates of amorphous $Ga(OH)_3$ were obtained in the absence of the dipeptide. This study suggests that a designed peptide with an active functionality can be further exploited to produce inorganic compounds with controlled nucleation and growth.

Iron oxide biomineralization and applications

Learning the essence of magnetite biomineralization in bacteria

Magnetic particles are currently important materials in bioindustries.[64–66] They are widely used in medical and diagnostic

applications such as magnetic resonance imaging, cell separation, environmental inspections, drug delivery, and hyperthermia.[64,67] The major advantage of magnetic particles in such applications is that they can be easily manipulated by a magnetic force. Magnetic particles enable rapid and easy separation of target molecules bound to the magnetic particles from reaction mixtures. This technology is beneficial for use in fully automated systems, providing minimal manual labor and superior reproducibility.[64]

The presence of magnetic iron oxide in an organism was first discovered in the teeth of chitons, which are marine invertebrates.[5] Their teeth are coated with magnetite and are used to scrape microalgae off the substratum. After this finding, iron oxide minerals were further identified as small crystals in a wide range of organisms, including honey bees, fish, and birds.[9] In these organisms, the function of the iron oxide crystals is still under investigation, but they are suggested to function as biological compass needles to sense their locations through the earth's geomagnetic field. Magnetotactic bacteria have the ability to synthesize nano-sized single domain magnetite crystals (Fe_3O_4) that are aligned in a chain, enabling the cells to swim or to migrate along magnetic field lines (Fig. 6A and 6B). For the synthesis of magnetite crystals, the cells use a specialized intracellular membranous compartment, also referred to as a magnetosome.[68] The diameter of magnetosomes typically varies from 20 to 100 nm. The biomineralization process in magnetosomes is strictly controlled, leading to a highly regular and specific crystal size, shape, number, and assembly for a given bacterial strain. Recent studies on the molecular biology of magnetotactic bacteria have progressed our understanding of the formation mechanisms. Moreover, this knowledge provides insights into the potential use of magnetosomes, their proteins, and the bacterial cells as magnetic materials for biotechnological applications.[64]

After clarification of the complete genome sequence of magnetotactic bacteria (Fig. 6C and 6D),[69,70] tremendous improvements have been made in elucidating the molecular, biochemical, chemical and genetic bases of magnetosome formation and understanding how these unique intracellular organelles function. The genome information also allowed us to conduct comprehensive analyses of magnetotactic bacteria.[64,71,72] The experimental data obtained from the molecular studies with *Magnetospirillum* sp. suggested that magnetosomes are assembled in a step-wise manner in which membrane biogenesis, magnetosome protein localization, and biomineralization are placed under discrete genetic control (Fig. 7).[64,73,74] The first stage entails the invagination of the inner cell membrane to form a vesicle which serves as the precursor for magnetite crystals (Fig. 7A). The vesicles formed are assembled into a linear chain along with cytoskeletal filaments (Fig. 7B). Then, ferrous ions are accumulated into the vesicles through the transmembrane iron transporters (Fig. 7C). Internal iron is strictly controlled by an oxidation–reduction system. In the final stage, accumulated iron ions are crystallized within the vesicle (Fig. 7D). The formation and maintenance of membrane vesicles involves several proteins that might

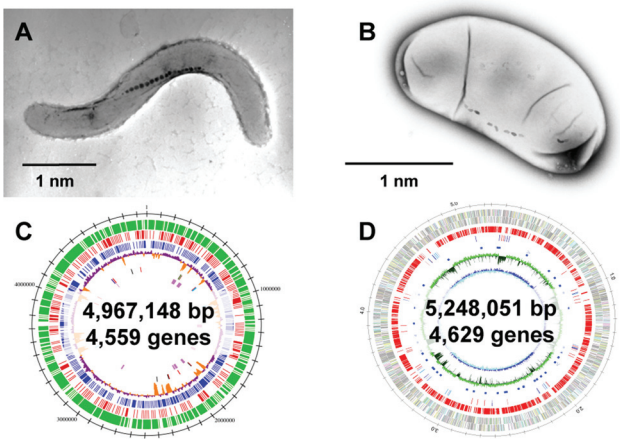

Fig. 6 Two representative strains of magnetotactic bacteria. Transmission electron microscopy (TEM) images of (A) *Magnetospirillum magneticum* strain AMB-1 and (B) *Desulfovibrio magneticus* strain RS-1. Reproduced with permission from ref. 64. Copyright 2008 Royal Society of Chemistry. (C) Genome feature of *Magnetospirillum magneticum* AMB-1. Reproduced with permission from ref. 69. Copyright 2005 Oxford University Press. (D) Genomic feature of *D. magneticus* RS-1. Reproduced with permission from ref. 70. Copyright 2009 Cold Spring Harbor Laboratory Press.

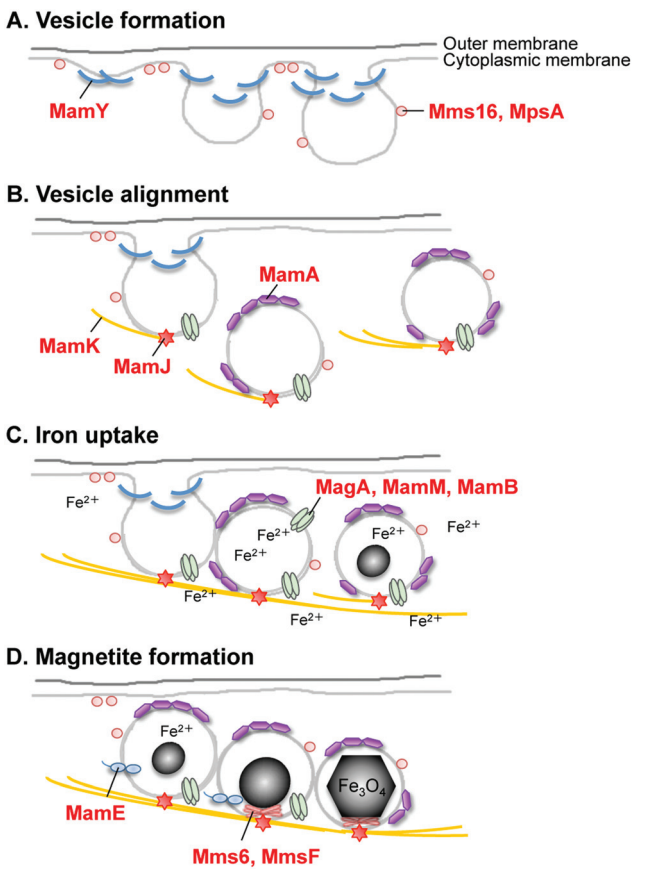

Fig. 7 Schematic for the hypothesized mechanism of magnetite biomineralization in magnetotactic bacteria.

be functionally associated or spatially co-localized together. The MamY protein was isolated from small magnetite crystals.[75] The MamY protein binds directly to the liposomes, causing formation of long tubules *in vitro*.[75] The function of the MamY protein is considered to involve the constriction of the magnetosome membrane during magnetosome vesicle formation. The MamA protein, which has a tetratricopepetide repeat (TPR) domain—a protein–protein interaction module—was identified as a dominant magnetosome membrane protein in *Magnetospirillum* sp.[76] Analysis of the crystal structure revealed that MamA folds as a sequential TPR protein with a unique hook-like shape.[77] MamA may act as a scaffold protein for magnetosome formation by interacting with other magnetosome-forming proteins. Mms16 and MpsA proteins are speculated to prime the invagination site of the cytoplasmic membrane for vesicle formation.[78] MagA is a proton-driving H^+/Fe^{2+} antiporter protein.[79] MamM, a cation diffusion facilitator family protein, is a multifunctional protein involved in the crystallization, initiation, and regulation of proper localization of other magnetosome proteins.[80] MamB, which also exhibits similarity to the cation diffusion facilitator family, was observed to interact with several other proteins, including the PDZ1 domain of MamE.[81] MamP is an iron oxidase that contributes to the magnetite crystal growth.[82] MamK is a homolog of the bacterial actin-like protein, and has been shown to form filaments to establish the chain-like structure of magnetosomes through appropriate subcellular targeting.[83] MamJ is an acidic protein associated with the MamK filament, and it directs the assembly of the magnetosome chain.[84]

A key protein that regulates the morphology of cubo-octahedral magnetite crystals was isolated in a study on the *M. magneticum* strain AMB-1 (Table 1).[17] The Mms6 protein (Fig. 7D) represents a class of proteins that are tightly associated with the magnetite crystals. Three other proteins, designated as Mms5 (MamG), Mms7 (MamD), and Mms13 (MamC), were also isolated along with the Mms6 protein. Mms5, Mms6, and Mms7 showed a common amphiphilic characteristic containing hydrophobic N-terminal and hydrophilic C-terminal regions and could be categorized into a family of proteins. The N-terminal regions in Mms5, Mms6, and Mms7 possess a common leucine and glycine repetitive sequence. These amino acid sequences did not show any similarity to known proteins found in other organisms, suggesting that these proteins are specific in magnetotactic bacteria. Following competitive iron-binding analysis with other inorganic cations, it has been suggested that the C-terminal region is an iron-binding site.[17] The N-terminal region is responsible for the self-aggregation of this protein.[85,86] These characteristics are considered to contribute to magnetite biomineralization in bacteria.

The function of the Mms6 protein in bacterial cells was elucidated by the analysis of the gene deletion mutant *mms6* (Fig. 8). Surprisingly, the *mms6* deletion mutant synthesized smaller and irregular-shaped magnetite crystals (Fig. 8B), while the wild-type and complementation strains produced highly ordered cubo-octahedral crystals (Fig. 8A).[87] Uncommon crystal faces, such as {210}, {211}, and {311}, were detected in

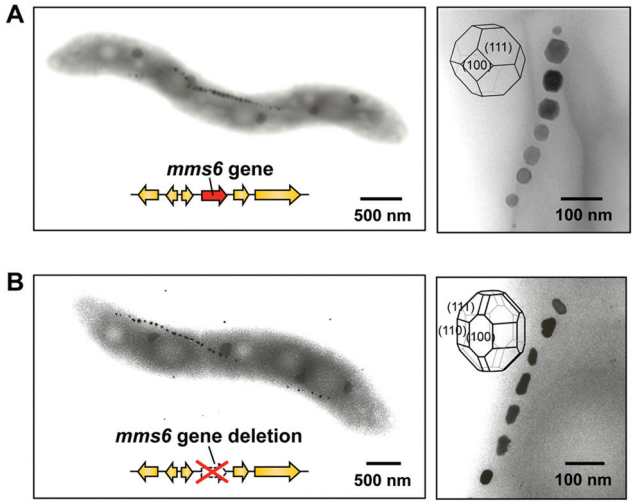

Fig. 8 Elucidation of the function of the Mms6 protein in *Magnetospirillum magneticum* AMB-1 using gene deletion. (A) The wild-type strain synthesized highly ordered cubo-octahedral crystals. (B) The *mms6* gene deletion mutant synthesized smaller magnetite crystals with uncommon crystal faces. Reproduced with permission from ref. 87. Copyright 2011 American Society for Biochemistry and Molecular Biology.

magnetite crystals from the *mms6* deletion mutant, in contrast to the cubo-octahedral magnetite crystals in wild-type and complementation strains, which had {111} and {100} crystal faces. These results indicate that the Mms6 protein regulates crystal surfaces to control the magnetite crystal morphology during crystal growth in magnetotactic bacterial cells. In addition, Mms5, Mms7, and Mms13 have similar but different functions from the Mms6 protein, and they cooperate in the formation of magnetites of consistent crystal size and morphology.[88] This is the first example of a protein being involved in the regulation of a nano-sized crystallographic structure in *in vivo* biomineralization.

Application of magnetite biomineralization proteins for magnetite synthesis

Particle size and morphology are important factors for the use of magnetites in practical applications because they strongly affect magnetic properties.[67] The development of reliable and reproducible methods that enable synthesis of magnetic particles with controlled size and morphology has therefore been a major challenge in this field over the years.[89] Given the increasing demand for magnetic nano-materials, alternative processes for the simple formation of size- and shape-controlled magnetite crystals in the aqueous environment are required.

Biomimetic approaches that use the function of the Mms6 protein (Table 1) for preparing magnetite crystals have been investigated using two synthetic methods.[17,85,90] Co-precipitation of ferrous and ferric ions in the presence of Mms6 produced uniform magnetite crystals with sizes ranging from 20 to 30 nm, while the absence of the protein resulted in the formation of crystals with irregular morphologies and sizes.[17]

The result suggests that Mms6 mediates crystal formation by binding precursors and/or magnetite crystals to regulate morphology. Prozorov *et al*. applied this synthetic method for the production of cobalt ferrite ($CoFe_2O_3$).[91]

Alternatively, a method involving partial oxidation of ferrous hydroxide in the presence of Mms6 was employed (Fig. 9).[85] Mms6-mediated synthesis of magnetites by this method produced crystals of uniform size with narrow size distribution (approximately 20 nm in diameter) and a cubo-octahedral morphology consisting of {111} and {100} crystal faces (Fig. 9A and 9C). The crystal surfaces were similar to those of magnetosomes observed in the *M. magneticum* strain AMB-1. In contrast, the crystals formed in the absence of Mms6 were octahedral, consisting of {111} crystal faces, which were larger and had increased size distribution (approximately 30 nm in diameter) (Fig. 9B and 9D). Protein quantification analysis of Mms6 in the synthesized crystals indicated tight association of this protein with the crystal.[85]

Short synthetic peptides that mimicked the characteristic amino acid sequences of Mms6 were further investigated for the synthesis of magnetite crystals (Fig. 9E).[90] Magnetite synthesis using M6A peptides containing the C-terminal acidic region of Mms6 resulted in the formation of particles with a cubo-octahedral morphology similar to those of magnetosomes and particles formed in the presence of the Mms6 protein. Shape-regulated cobalt-doped magnetite nanoparticles were also synthesized through this method.[92] High magnetic saturation, high coercivity magnetic particles with a narrow size distribution in the single-domain size can be produced by optimizing the conditions of the protein-mediated synthetic method.

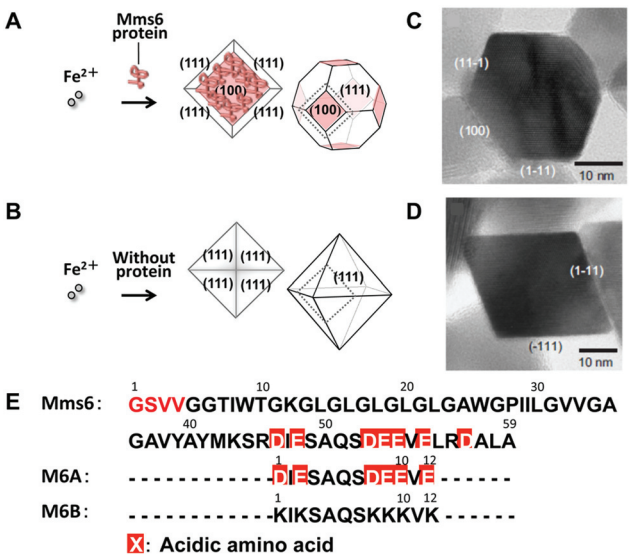

Fig. 9 Schematic illustrations of magnetic particles synthesized (A) with or (B) without Mms6. TEM images of magnetic particles synthesized (C) in the presence of Mms6 and (D) in the absence of the Mms6 protein. Reproduced with permission from ref. 85. Copyright 2007 Elsevier. (E) Amino acid sequences of Mms6, M6A, and M6B. D: aspartic acid and E: glutamic acid.

Magnetite formation using Mms6 was also exploited to synthesize magnetic particles on planar substrates by bottom-up approaches.[93,94] A silicon substrate was modified with a self-assembled monolayer of octadecyltrimethoxysilane and the Mms6 protein through hydrophobic interactions between the protein molecules and the monolayer. Active carboxylic groups of the Mms6 protein are arranged on the surface of substrates. The crystals were selectively formed in the specific regions modified with the Mms6 protein.[93] Galloway *et al*. applied a soft-lithographic technique to fabricate surface patterning of the Mms6 protein and used it for the formation of biomimetic magnetite nanoparticle arrays.[94] Nanocrystals of magnetites were successfully formed on the patterned surface. These methods offer an alternative strategy for magnetite formation under mild conditions and could be used for construction of high-density data storage.

Calcium carbonate biomineralization and applications

Learning the essence of calcium carbonate biomineralization

Calcium carbonate ($CaCO_3$) is one of the most abundant inorganic compounds in biominerals. Mollusk shells, exoskeletons of crustaceans, coccolith of coccolithophores, and egg shells consist of $CaCO_3$.[2] Three different polymorphs, calcite, aragonite, and vaterite, are well-characterized in crystalline $CaCO_3$. Amorphous calcium carbonate,[95–98] which is observed in the cuticle of the exoskeleton of crustaceans, is also recognized. A typical example of the controlled $CaCO_3$ hybrid structure is the nacre of the abalone shell (Fig. 10A, left).[2] Plate-like aggregates of nanocrystalline aragonite submicrometer in thickness showing uniaxial crystallographic orientation are formed between the pre-organized macromolecular sheets (Fig. 10B). The stacks of the $CaCO_3$ tablets, having uniform

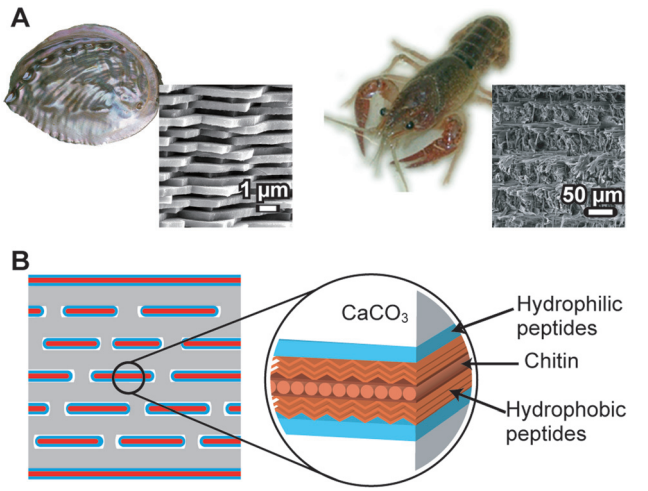

Fig. 10 (A) Calcium carbonate ($CaCO_3$)-based biominerals; left: abalone shell; right: the exoskeleton of crayfish. Insets show SEM images of biominerals. (B) Schematic of the nacre of the abalone shell.

thickness, provide structural colors on the pearl's surface. The exoskeleton of crayfish is also an example of a $CaCO_3$-based biomineral (Fig. 10A, right). The exoskeleton mainly consists of α-chitin/protein microfibril frameworks, and both calcite and amorphous calcium carbonate are closely associated with the fibrils. Mollusk shells and the exoskeletons of crustaceans are fascinating biominerals from a materials science perspective because they are tough and lightweight.[6]

Similar to other biominerals described in previous sections, organic biopolymers in the form of proteins, glycoproteins, and polysaccharides are proposed to play main roles in the $CaCO_3$ biomineralization processes.[2,12–16] The biopolymers control the formation of minerals with uniform crystal size, nanostructural regularity, specific crystallographic phase, morphologies, and orientations. The highly organized and hierarchical structures with the organic/inorganic composition of the minerals achieve fracture resistance. To date, many proteins have been identified from different organisms or species forming $CaCO_3$ biominerals.[12–16] Materials scientists have been inspired by these molecularly controlled processes,[21–25,99–103] although some of the formation mechanisms are yet unclear. In this section, we describe synthetic approaches for the formation of $CaCO_3$/polymer hybrids as templates.

Inspired by the roles of biomacromolecules in biomineralization, synthetic systems for the formation of $CaCO_3$/polymer hybrids have been developed.[104–111] Thin-film hybrids have been obtained by the cooperative effects of polymer film matrices and soluble additives of acidic polymers. Fig. 11 shows a schematic representation of the formation of these hybrids, and their polarized optical microscopy and scanning electron microscopy (SEM) images. Spin-coated thin films of polysaccharides, such as chitin[104,105] and chitosan[106–108] on glass substrates, were used as insoluble templates. Thin-film $CaCO_3$ with flat surfaces developed on the insoluble organic templates in the presence of acidic polymers such as poly(acrylic acid) (PAA), poly(aspartic acid), and poly(glutamic acid) until the polymer film was fully covered with $CaCO_3$. The functional groups forming H-bonds, such as –OH and –NH groups on the surface of the organic matrix, interact with the acidic group of the soluble polymer additive.[109] Then, acidic macromolecules induce a locally high concentration of calcium ions, resulting in the nucleation of crystalline thin films. Their polymorphs are calcite, which is the thermodynamically most stable state, and vaterite, which is the kinetically preferred state. These films are composed of assembled nanocrystals with radially oriented *c* axes, as revealed from the polarized optical microscopy image showing crossed extinction between the polarizers (Fig. 11). The supramacromolecules also act as soluble polymer additives, which have polyrotaxane structures composed of acidic cyclodextrins and polyethylene oxide.[112]

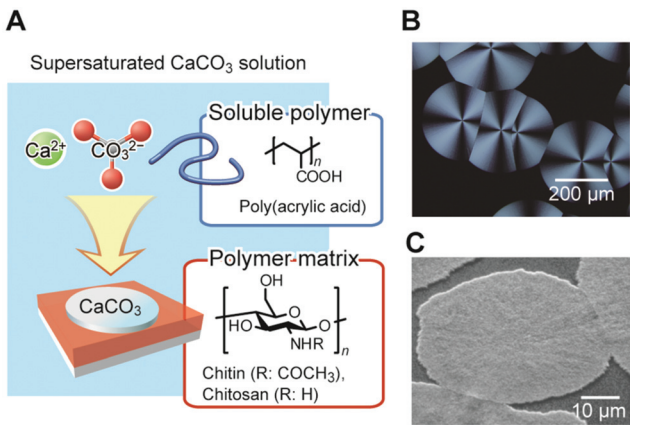

Fig. 11 (A) Schematic illustration of the formation of thin-film $CaCO_3$/organic hybrids. Reproduced with permission from ref. 100. Copyright 2010 Cambridge University Press. (B) Polarized optical microscopy image of a thin-film hybrid developed on a chitosan matrix in the presence of poly(acrylic acid). (C) Scanning electron microscopy image of $CaCO_3$ hybrids formed on the chitin matrix. Reproduced with permission from ref. 104. Copyright 2000 The Chemical Society of Japan.

Cooperative effects between soluble bio-macromolecules and the polysaccharide film matrices enable highly controlled crystallization of $CaCO_3$ in synthetic systems. One of the peptides (CAP-1) involved in $CaCO_3$ biomineralization was isolated from the exoskeleton of crayfish (Table 1) and used in soluble additives in a crystallization experiment in order to understand the structure–function relationships of the peptide.[113] CAP-1 is a highly acidic peptide, which has interesting structural features (Fig. 12A). In particular, it has a six consecutive aspartate sequence at the C terminal. The chitin-binding motif, called the Rebers–Riddiford consensus sequence, is seen at the central part of CAP-1. This consensus sequence is found in many cuticle proteins in crustaceans and considered to be involved in binding to the crystalline structure of chitin.[114] The serine at the 70th position of CAP-1 was phosphorylated, which may bind to calcium ions and stabilize the $CaCO_3$ amorphous precursors.[99,115]

In the presence of CAP-1, unidirectionally oriented thin-films of $CaCO_3$/chitin hybrids, approximately on the ten-micrometer scale, were obtained on the matrix (Fig. 12B, right).[113] These thin films are assemblies of nanocrystals of about 100 nm in size with single-crystal orientation. No oriented crystals are obtained on a glass substrate or on an amorphous chitosan matrix in the presence of CAP-1 (Fig. 12C). The cooperative interaction of each CAP-1 functional part induces the formation of the unidirectionally oriented $CaCO_3$ thin film crystals on chitin fibrils. The $CaCO_3$ amorphous precursors stabilized with CAP-1 are initially formed on the chitin fibrous matrix. The alignment of the functional groups of CAP-1 binding on the crystalline chitin fibrils induces the nucleation of $CaCO_3$ in the deposited amorphous precursors.[113] Analogous recombinant peptides of CAP-1 have been synthesized and used as additives for crystallization of $CaCO_3$ to examine the effects of each functional part on $CaCO_3$ crystal growth.[116–118] The crystallographic orientation depends on the chitin-binding consensus sequence (the Ribers–Riddiford consensus sequence), and the functional group of the 70th residue is critical to the surface morphology of thin-film crystals.

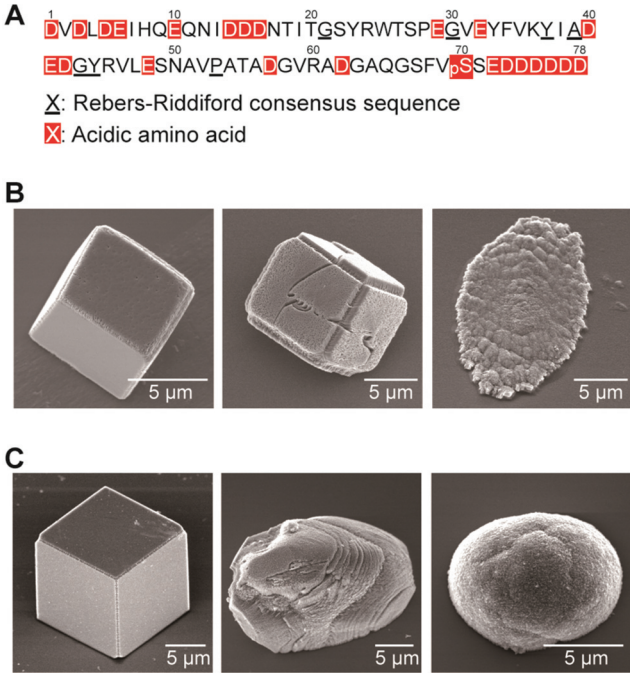

Fig. 12 (A) Amino acid sequence of the CAP-1 peptide isolated from the exoskeleton of crayfish. Amino acid sequence; D: aspartic acid; E: glutamic acid; pS: phosphoserine. (B) Scanning electron microscopy (SEM) images of $CaCO_3$ crystals formed on chitin matrices in the presence of CAP-1. (C) SEM images of $CaCO_3$ crystals formed on glass substrates in the presence of CAP-1. B, (C) Concentrations of CAP-1: 3.0×10^{-4} wt% (left): 1.0×10^{-3} wt% (center); 3.0×10^{-3} wt% (right). Reproduced with permission from ref. 113. Copyright 2006 Wiley-VCH Verlag GmbH & Co. KGaA.

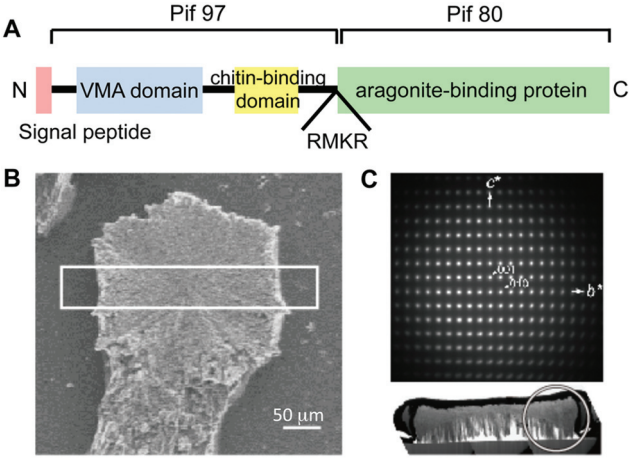

Fig. 13 (A) Schematic illustration of the overall protein structure of the Pif complex. Red, blue, and yellow boxes represent the signal peptide, VWA domain, and peritrophin A-type chitin-binding domain, respectively. RMKR is a Kex2-like proteinase cleavage site. Green box is the aragonite-binding protein (Pif 80). (B) A fragment of the $CaCO_3$ crystal observed by SEM. (C) Electron diffraction pattern of the white circled area in the cross-section of the white box in (B), indicating a single aragonite crystal and its *c* axis perpendicular to the glass plate. Reproduced with permission from ref. 14. Copyright 2009 American Association for the Advancement of Science.

The matrix proteins Pif80 and Pif97 were isolated from the pearl oyster *P. fucata* by Suzuki, Nagasawa, and coworkers[14] (Table 1). Pif80 and Pif97 form a Pif complex *in vivo via* disulfide bonds (Fig. 13A). The Pif complex plays key roles in controlling $CaCO_3$ crystallization for the formation of the nacreous layers. It was found that the Pif complex works on the interface between the organic framework and aragonite through an aragonite-binding domain in Pif80 and a chitin-binding domain in Pif97. These domains allow the organic framework and calcium carbonate crystals to interact. When the Pif complex is used as a soluble additive for calcium carbonate crystallization on the chitin matrix *in vitro*, the Pif complex induces the aragonite thin film with the *c* axis unidirectionally aligned perpendicular to the surface, as observed for natural nacre (Fig. 13B and 13C).

Application of calcium carbonate biomineralization mechanisms toward the formation of functional hybrids

In the biomimetic synthesis of $CaCO_3$, designed templates and/or additives with specific functional groups have been used for the preparation of organic/inorganic hybrids.[21–25,99–103] $CaCO_3$ crystals with controlled polymorphs and crystallographic orientations are formed on insoluble templates such as self-assembled monolayers (SAMs)[21,119] and polymer brushes.[120–123] The use of soluble polymers, containing acidic functional groups such as carboxyl groups and phosphate groups that interact with inorganic substances, leads to the formation of a variety of complex structures.[99–103,124–127] The experimental and simulation studies on the $CaCO_3$ precursor stabilized by magnesium ions was also performed to reveal the formation mechanism of the hybrids.[128,129] In this section, we focus on the hybrids of $CaCO_3$, and synthetic and semi-synthetic polymers obtained by cooperative effects between film matrices and soluble additives.

A significant aspect of biomineralization is that crystallization is precisely controlled by templates of aligned polymers. As mentioned above, well-controlled oriented aragonite nanocrystals are formed in the nacre of the abalone shell.[2,6] Preparation of such controlled crystal structures is still challenging for the present technology, and both synthetic and biological approaches are needed. As a synthetic approach, the use of a crystalline poly(vinyl alcohol) (PVA) matrix leads to the induction of aragonite crystallization in the presence of PAA.[110] The polycrystalline PVA matrix is prepared by annealing a spin-coated PVA film. The lattice of the PVA (100) face matches the aragonite lattice. It is considered that the PAA interacting with the hydroxy groups in the micro-domains of the crystalline PVA forms the local arrangement of carboxylic acid groups. These aligned carboxylates locally arrange the calcium ions, leading to the nucleation of aragonite. The distance between the functional groups on the PAA polymer backbone is the same as that for PVA, resulting in the selective formation of aragonite. In contrast, the use of poly(glutamic acid) (PGA) as a soluble additive leads to the formation of thin-film vaterite on the PVA matrix because of different distances between the functional groups.[110]

Unidirectionally oriented polymer/$CaCO_3$ hybrids were obtained using macroscopically oriented polymer matrices through macromolecular templating in the presence of simple acidic polymers.[130] Fig. 14 shows polarized optical microscopy images of the oriented chitin matrix, made from chitin phenylcarbamate, forming lyotropic liquid-crystalline (LC) structures and the calcite crystals grown on the oriented matrix. The LC chitin derivatives were synthesized by the carbamation of chitin (Fig. 14A). The condensed solution of LC chitin derivatives was converted to the gel state by soaking in methanol. The gel was oriented by stretching. After cleavage by hydrolysis of the carbamate groups, the oriented chitin matrix was obtained (Fig. 14B) and immersed in a crystallization solution for the controlled crystal growth of $CaCO_3$. Rod-shaped crystals were grown for 15 h to about 80 μm in the ordered chitin matrix and aligned parallel to the direction of the polymer main chains of the matrix (Fig. 14C). When polarized optical microscopy is used, the visibility of the rod crystals oscillates between bright and dark with every 45° rotation, as shown in Fig. 14D. This indicates that the crystallographic orientation of the rod crystals corresponds to the longitudinal axis of the rod crystals. The SEM images of the isolated $CaCO_3$ rods (Fig. 14E) indicate that the rod crystals formed on the oriented matrix are assemblies of rhombohedral calcite crystals with fine facets of approximately 500 nm in size. Moreover, TEM images and the corresponding electron diffraction patterns of the selected area show that the rod calcite has a single crystalline orientation (Fig. 14F). The crystals exhibiting such features are categorized as mesocrystals.[126,127,131] LC polymers are useful for control of oriented structures from the macroscopic to molecular levels. In nature, the silkworm cocoon and the exoskeleton of the jewel beetle also have a precisely ordered hierarchical structure. It is considered that these hierarchical structures are formed *via* liquid crystalline structures.[132,133] This LC methodology may provide novel ways towards the development of hybrids with oriented structures based on functional inorganic crystals.[134]

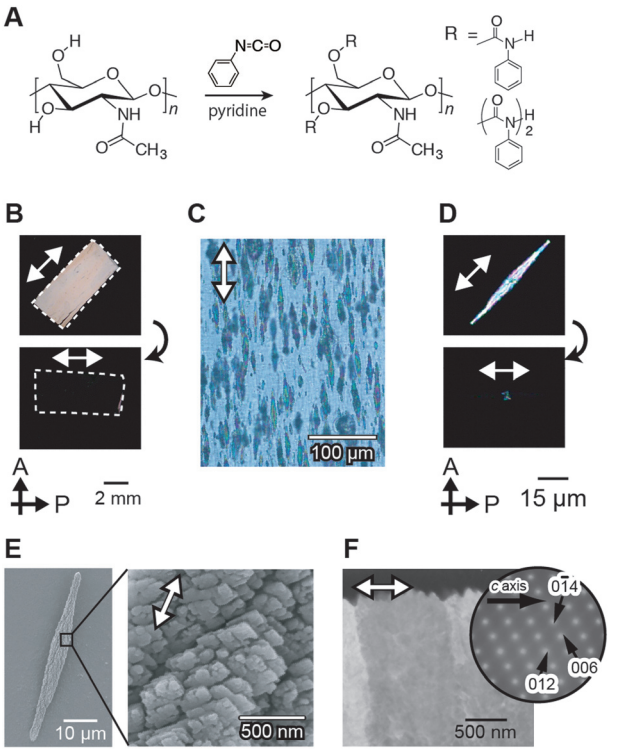

Fig. 14 Macroscopically ordered $CaCO_3$/organic hybrids grown on ordered macromolecular templates. (A) Synthetic scheme of chitin phenylcarbamate. Polarized optical microscopy images of (B) an oriented template, (C) the hybrids obtained, and (D) isolated $CaCO_3$ crystals. (E) SEM images of the $CaCO_3$ crystals. (F) TEM image of cross-sections of $CaCO_3$ crystals. Reproduced with permission from ref. 130. Copyright 2008 Wiley-VCH Verlag GmbH & Co. KGaA.

Stiff, flexible, elastic, and transparent bulk materials are designed and synthesized by mimicking the structure of crustacean exoskeletons (Fig. 15).[135] These elastic nanocomposite materials are prepared from a bulk matrix consisting of amorphous calcium carbonate and poly(acrylic acid), and reinforcing cellulose nanofibers. These unique characteristics cannot be obtained by simple mixing of cellulose and calcium carbonate. The strong interactions at the interface between the surface of the cellulose nanofibers and calcium carbonate are keys for these properties. The cellulose nanofiber matrix oxidized by the TEMPO-mediated system on the surface is used because carboxyl groups form on the surface of the nanofibers. Moreover the carboxylate group of the poly(acrylic acid) and the hydroxyl groups of cellulose interact at the interface of the bulk amorphous calcium carbonate and cellulose.

Not only the polymorphs of the $CaCO_3$ films, but also the morphologies of the hybrids are affected by the polymer matrices. Film hybrids with regular surface-relief structures self-organize when "soft" hydrogel film matrices are used.[111] A pullulan derivative, with the main chain of a water-soluble polysaccharide and hydrophobic cholesteryl groups as non-covalent crosslinking points, has been reported to form a physical hydrogel in aqueous solution. In this hydrogel matrix, $CaCO_3$ crystals develop inside the gel in the presence of PAA as a thin-film hybrid with regular surface-relief structures. The period of the patterned relief structures ranges from sub-micrometers to a few micrometers. It is considered that the formation of patterned thin films is induced by spontaneous oscillation of the ion concentrations because of slow ion diffusion in the gels.

$CaCO_3$ crystals with complex structures are self-organized by the cooperative effects between matrices of PVA derivatives in the presence of soluble additives (Fig. 16).[136–140] PVA derivatives can also form "soft" and "hard" hydrogels as thin-film matrices depending on the degree of crosslinking. The hydrogel matrix is obtained by thermal treatment of a PVA-based copolymer and the properties of the gel matrices are altered by the thermal procedures. On the "soft" hydrogel matrix of PVA, thin-film hybrids with patterned surface structures are obtained.[136]

When we use a more cross-linked "hard" PVA hydrogel as a matrix for the crystal growth, three dimensional (3D) patterned relief objects, on the scale of about tens of micrometers, are

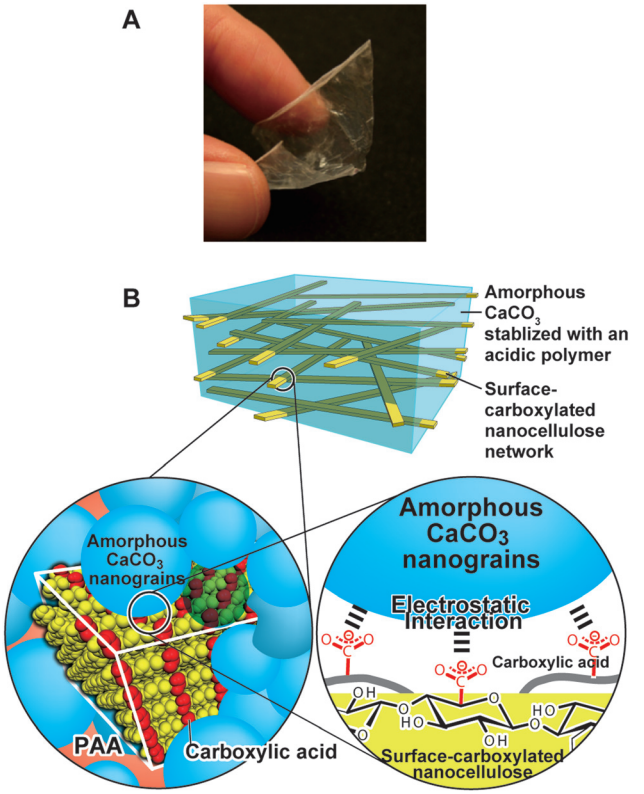

Fig. 15 (A) Elastic flexibility of the nanocellulose/ACC composites and (B) schematic illustration of the composites. Reproduced with permission from ref. 135. Copyright 2014 Royal Society of Chemistry.

formed in the presence of PAA (Fig. 16A and 16B).[137] The 3D structures are formed in two steps and are different from the relief structures of the thin-film crystals. The first step is the formation of thin-film $CaCO_3$ hybrids with a flat surface (Fig. 16A). These film crystals show concentric dark rings under crossed polarizers. In this flat film of $CaCO_3$, the directions of the *c* axes for the $CaCO_3$ crystals change periodically between the perpendicular orientation and the parallel orientation to the direction of the crystal growth. The self-organized periodic orientation in this first step results from diffusion-controlled crystal growth. The second step is the formation of the 3D relief objects composed of needle-like $CaCO_3$ crystals on the flat surface of the template (Fig. 16B). The height of the relief objects is about 5 μm and the period is about 10 μm. The needle-like $CaCO_3$ crystals are self-assembled into the micrometer-scale relief objects. These 3D-structured $CaCO_3$ crystals can be used as substrates for cultivation of pre-osteoblastic cells.[140] The ordered microgrooves enhanced adhesion, spreading, proliferation, and differentiation of the cells. X-ray diffraction studies of the relief objects show that in the ridge regions, the *c* axes of the needle-like crystals are aligned perpendicularly to the substrate. The crystals formed in the second step have the same orientation as those in the underlying thin film.[137] These results indicate that the flat thin-film crystals formed in the first step serve as templates in the

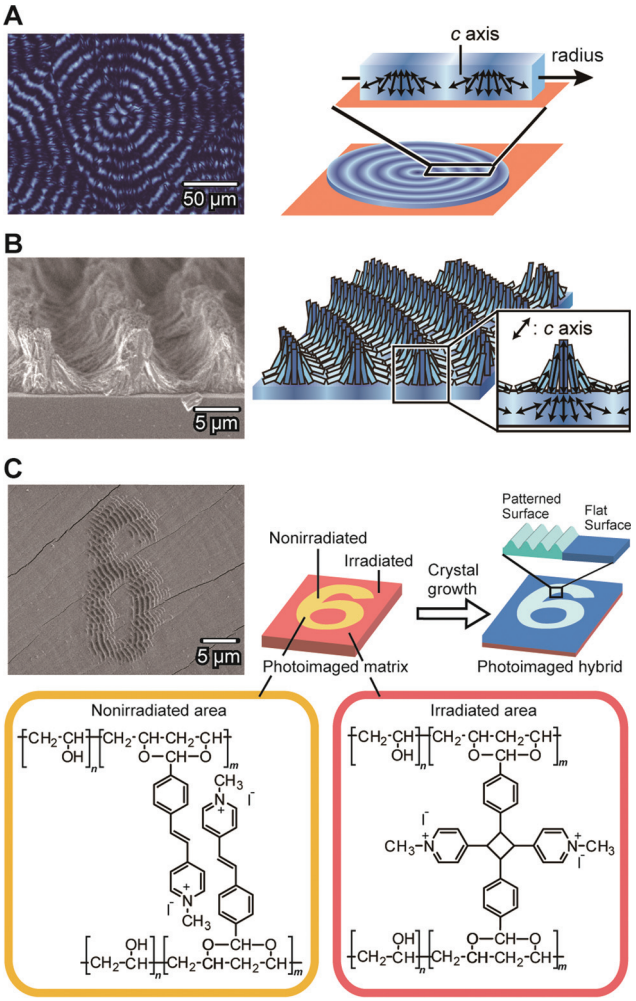

Fig. 16 Self-organization of $CaCO_3$ crystals with complex structures. (A) Thin-film showing periodic crystallographical orientations. Left: polarized optical microscopy image; right: schematic illustration of the structure. (B) Three-dimensional structures formed on the thin film shown in (A). Left: SEM image; right: schematic illustration of the structure. Reproduced with permission from ref. 137. Copyright 2009 American Chemical Society. (C) Photoimaged $CaCO_3$/polymer hybrid films formed on the matrix of the photoreactive PVA-derivative. Upper left: SEM image; upper right: schematic illustration of the formation process; bottom: chemical structures of the photoreactive PVA-derivative. Reproduced with permission from ref. 138. Copyright 2011 Wiley-VCH Verlag GmbH & Co. KGaA.

second step. In addition, the flat-film template also induces regular architectures for different kinds of carbonate crystals such as $SrCO_3$.

Tuning the degree of cross-linking in the polymer matrix using photoreactions allows for photoimaging of $CaCO_3$ hybrid films with self-organized structures (Fig. 16C).[138] Figures written on a photoreactive polymer film were transferred into $CaCO_3$ crystal morphologies. The $CaCO_3$ crystal films with microscopic regular relief structures and flat surfaces are self-organized on the non-irradiated and UV-irradiated areas of the matrix, respectively. As a result, the hierarchically ordered polymer/$CaCO_3$ hybrid films are formed

through the combination of the top-down photoimaging method and the bottom-up self-organization method.

Conclusions

The results obtained from fundamental studies on biomineralization have allowed us to develop various organic/inorganic hybrid materials using proteins isolated from organisms and/or their mimicking macromolecules. Although biomineralization mechanisms in most biological systems are extremely complicated, current biomimetic and bio-inspired syntheses are based on only certain aspects of these mechanisms. The application of various synthetic routes using multiple molecules will enable tuning of the crystal size, morphology, surface structures, composition, crystallinity, and even hierarchical organization of materials. These principles will also facilitate the development of functional organic/inorganic hybrid materials with multiple combinations of outstanding properties including lightweight, high flexibility, mechanical strength, dynamic function and structural hierarchy through environmentally benign routes. More advanced materials will be created in the future for a wide array of tailor-made applications *via* collaborative work between researchers in a wide variety of scientific fields, including inorganic chemistry, organic chemistry, biology, computer science and engineering.

Acknowledgements

This work was partially supported by a Grant-in-Aid for Scientific Research (KAKENHI) on Innovative Areas of "Fusion Materials: Creative Development of Materials and Exploration of Their Function through Molecular Control" (no. 2206) from the Ministry of Education, Culture, Sports, Science and Technology, Japan (MEXT).

Notes and references

1 S. V. Dorozhkin and M. Epple, *Angew. Chem., Int. Ed.*, 2002, **41**, 3130–3146.
2 S. Weiner and L. Addadi, *J. Mater. Chem.*, 1997, **7**, 689.
3 N. Kroeger, R. Deutzmann and M. Sumper, *Science*, 1999, **286**, 1129.
4 K. Shimizu, J. Cha, G. D. Stucky and D. E. Morse, *Proc. Natl. Acad. Sci. U. S. A.*, 1998, **95**, 6234.
5 H. A. Lowenstam, *Geol. Soc. Am. Bull.*, 1962, **73**, 435.
6 M. A. Meyers, J. McKittrick and P. Y. Chen, *Science*, 2013, **339**, 773.
7 J. C. Weaver, G. W. Milliron, A. Miserez, K. Evans-Lutterodt, S. Herrera, I. Gallana, W. J. Mershon, B. Swanson, P. Zavattieri, E. DiMasi and D. Kisailus, *Science*, 2012, **336**, 1275.
8 J. Aizenberg, A. Tkachenko, S. Weiner, L. Addadi and G. Hendler, *Nature*, 2001, **412**, 819.
9 C. E. Diebel, R. Proksch, C. R. Green, P. Neilson and M. M. Walker, *Nature*, 2000, **406**, 299.
10 J. Aizenberg, V. C. Sundar, A. D. Yablon, J. C. Weaver and G. Chen, *Proc. Natl. Acad. Sci. U. S. A.*, 2004, **101**, 3358.
11 F. Natalio, T. P. Corrales, M. Panthoefer, D. Schollmeyer, I. Lieberwirth, W. E. G. Mueller, M. Kapp, H. J. Butt and W. Tremel, *Science*, 2013, **339**, 1298.
12 I. M. Weiss, S. Kaufmann, K. Mann and M. Fritz, *Biochem. Biophys. Res. Commun.*, 2000, **267**, 17.
13 S. Sudo, T. Fujikawa, T. Nagakura, T. Ohkubo, K. Sakaguchi, M. Tanaka, K. Nakashima and T. Takahashi, *Nature*, 1997, **387**, 563.
14 M. Suzuki, K. Saruwatari, T. Kogure, Y. Yamamoto, T. Nishimura, T. Kato and H. Nagasawa, *Science*, 2009, **325**, 1388.
15 R. Lakshminarayanan, R. Kini and S. Valiyaveettil, *Proc. Natl. Acad. Sci. U. S. A.*, 2002, **99**, 5155.
16 H. Inoue, N. Ozaki and H. Nagasawa, *Biosci., Biotechnol., Biochem.*, 2001, **65**, 1840.
17 A. Arakaki, J. Webb and T. Matsunaga, *J. Biol. Chem.*, 2003, **278**, 8745.
18 J. N. Cha, K. Shimizu, Y. Zhou, S. C. Christiansen, B. F. Chmelka, G. D. Stucky and D. E. Morse, *Proc. Natl. Acad. Sci. U. S. A.*, 1999, **96**, 361.
19 R. L. Brutchey, E. S. Yoo and D. E. Morse, *J. Am. Chem. Soc.*, 2006, **128**, 10288.
20 D. Kisailus, Q. Truong, Y. Amemiya, J. C. Weaver and D. E. Morse, *Proc. Natl. Acad. Sci. U. S. A.*, 2006, **103**, 5652.
21 J. Aizenberg, A. J. Black and G. M. Whitesides, *Nature*, 1999, **398**, 495.
22 H. Imai, Y. Oaki and A. Kotachi, *Bull. Chem. Soc. Jpn.*, 2006, **79**, 1834.
23 T. Kato, A. Sugawara and N. Hosoda, *Adv. Mater.*, 2002, **14**, 869.
24 F. C. Meldrum and H. Coelfen, *Chem. Rev.*, 2008, **108**, 4332.
25 F. Nudelman and N. A. J. M. Sommerdijk, *Angew. Chem., Int. Ed.*, 2012, **51**, 6582.
26 T. L. Simpson and B. E. Volcani, *Silicon and Siliceous Structures in Biological Systems*, Springer-Verlag, New York, USA, 1981.
27 N. Kroger, R. Deutzmann, C. Bergsdorf and M. Sumper, *Proc. Natl. Acad. Sci. U. S. A.*, 2000, **97**, 14133.
28 S. Matsunaga, R. Sakai, M. Jimbo and H. Kamiya, *ChemBioChem*, 2007, **8**, 1729.
29 H. Ehrlich, R. Deutzmann, E. Brunner, E. Cappellini, H. Koon, C. Solazzo, Y. Yang, D. Ashford, J. Thomas-Oates, M. Lubeck, C. Baessmann, T. Langrock, R. Hoffmann, G. Worheide, J. Reitner, P. Simon, M. Tsurkan, A. V. Ereskovsky, D. Kurek, V. V. Bazhenov, S. Hunoldt, M. Mertig, D. V. Vyalikh, S. L. Molodtsov, K. Kummer, H. Worch, V. Smetacek and M. J. Collins, *Nat. Chem.*, 2010, **2**, 1084.
30 J. C. Weaver and D. E. Morse, *Microsc. Res. Tech.*, 2003, **62**, 356.

31 X. Wang, L. Gan, K. P. Jochum, H. C. Schroeder and W. E. G. Mueller, *Evid. Based Complementary Altern. Med.*, 2011, **2011**, 1.
32 V. B. Kozhemyako, G. N. Veremeichik, Y. N. Shkryl, S. N. Kovalchuk, V. B. Krasokhin, V. A. Rasskazov, Y. N. Zhuravlev, V. P. Bulgakov and Y. N. Kulchin, *Mar. Biotechnol.*, 2010, **12**, 403.
33 A. Krasko, B. Lorenz, R. Batel, H. C. Schroeder, I. M. Mueller and W. E. G. Mueller, *Eur. J. Biochem.*, 2000, **267**, 4878.
34 W. E. G. Mueller, U. Schlossmacher, C. Eckert, A. Krasko, A. Boreiko, H. Ushijima, S. E. Wolf, W. Trernel, I. M. Mueller and H. C. Schröder, *Eur. J. Cell Biol.*, 2007, **86**, 473.
35 K. Mohri, M. Nakatsukasa, Y. Masuda, K. Agata and N. Funayama, *Dev. Dyn.*, 2008, **237**, 3024.
36 W. E. G. Mueller, C. Eckert, K. Kropf, X. H. Wang, U. Schlossmacher, C. Seckert, S. E. Wolf, W. Tremel and H. C. Schroeder, *Cell Tissue Res.*, 2007, **329**, 363.
37 W. E. G. Mueller, X. H. Wang, K. Kropf, A. Boreiko, U. Schlssmacher, D. Brandt, H. C. Schroeder and M. Wiens, *Cell Tissue Res.*, 2008, **333**, 339.
38 G. N. Veremeichik, Y. N. Shkryl, V. P. Bulgakov, S. V. Shedko, V. B. Kozhemyako, S. N. Kovalchuk, V. B. Krasokhin, Y. N. Zhuravlev and Y. N. Kulchin, *Mar. Biotechnol.*, 2011, **13**, 810.
39 Y. Zhou, K. Shimizu, J. N. Cha, G. D. Stucky and D. E. Morse, *Angew. Chem., Int. Ed.*, 1999, **38**, 780.
40 M. M. Murr and D. E. Morse, *Proc. Natl. Acad. Sci. U. S. A.*, 2005, **102**, 11657.
41 D. E. Morse, *Trends Biotechnol.*, 1999, **17**, 230.
42 R. L. Brutchey and D. E. Morse, *Chem. Rev.*, 2008, **108**, 4915.
43 W. E. G. Mueller, X. Wang, F.-Z. Cui, K. P. Jochum, W. Tremel, J. Bill, H. C. Schroeder, F. Natalio, U. Schloßmacher and M. Wiens, *Appl. Microbiol. Biotechnol.*, 2009, **83**, 397.
44 M. B. Dickerson, K. H. Sandhage and R. R. Naik, *Chem. Rev.*, 2008, **108**, 4935.
45 J. L. Sumerel, W. J. Yang, D. Kisailus, J. C. Weaver, J. H. Choi and D. E. Morse, *Chem. Mater.*, 2003, **15**, 4804.
46 D. Kisailus, J. H. Choi, J. C. Weaver, W. J. Yang and D. E. Morse, *Adv. Mater.*, 2005, **17**, 314.
47 I. Zlotnikov, P. Werner, H. Blumtritt, A. Graff, Y. Dauphin, E. Zolotoyabko and P. Fratzl, *Adv. Mater.*, 2014, **26**, 1682.
48 I. Fuchs, Y. Aluma, M. Ilan and Y. Mastai, *J. Phys. Chem. B*, 2014, **118**, 2104.
49 F. Natalio, T. P. Corrales, M. Panthöfer, D. Schollmeyer, I. Lieberwirth, W. E. G. Muller, M. Kappl, H.-J. Butt and W. Tremel, *Science*, 2013, **339**, 1298.
50 S. E. Wolf, U. Schlossmacher, A. Pietuch, B. Mathiasch, H. C. Schroeder, W. E. G. Mueller and W. Tremel, *Dalton Trans.*, 2010, **39**, 9245.
51 A. Rai and C. C. Perry, *J. Mater. Chem.*, 2012, **22**, 4790.
52 A. Polini, S. Pagliara, A. Camposeo, A. Biasco, H. C. Schroeder, W. E. G. Mueller and D. Pisignano, *Adv. Mater.*, 2011, **23**, 4674.
53 M. N. Tahir, P. Theato, W. E. G. Mueller, H. C. Schroeder, A. Borejko, S. Faiss, A. Janshoff, J. Huth and W. Tremel, *Chem. Commun.*, 2005, 5533.
54 M. N. Tahir, P. Theato, W. E. G. Mueller, H. C. Schroeder, A. Janshoff, J. Zhang, J. Huth and W. Tremel, *Chem. Commun.*, 2004, 2848.
55 M. N. Tahir, F. Natalio, H. A. Therese, A. Yella, N. Metz, M. R. Shah, E. Mugnaioli, R. Berger, P. Theato, H. C. Schroeder, W. E. G. Mueller and W. Tremel, *Adv. Funct. Mater.*, 2009, **19**, 285.
56 R. Andre, M. N. Tahir, H. C. C. Schroeder, W. E. G. Mueller and W. Tremel, *Chem. Mater.*, 2011, **23**, 5358.
57 M. I. Shukoor, F. Natalio, H. A. Therese, M. N. Tahir, V. Ksenofontov, M. Panthofer, M. Eberhardt, P. Theato, H. C. Schröder, W. E. G. Mueller and W. Tremel, *Chem. Mater.*, 2008, **20**, 3567.
58 B. Lange, N. Metz, M. N. Tahir, F. Fleischhaker, P. Theato, H. C. Schröder, W. E. G. Mueller, W. Tremel and R. Zentel, *Macromol. Rapid Commun.*, 2007, **28**, 1987.
59 O. V. Kaluzhnaya, S. I. Belikov, H. C. Schroeder, M. Wiens, M. Giovine, A. Krasko, I. M. Mueller and W. E. G. Mueller, *Naturwissenschaften*, 2005, **92**, 134.
60 F. Natalio, T. Link, W. E. G. Mueller, H. C. Schroeder, F. Z. Cui, X. H. Wang and M. Wiens, *Acta Biomater.*, 2010, **6**, 3720.
61 D. Kisailus, M. Najarian, J. C. Weaver and D. E. Morse, *Adv. Mater.*, 2005, **17**, 1234.
62 D. H. Adamson, D. M. Dabbs, C. R. Pacheco, M. V. Giotto, D. E. Morse and I. A. Aksay, *Macromolecules*, 2007, **40**, 5710.
63 I. Lee, J. Kwak, S. Haam and S. Y. Lee, *J. Cryst. Growth*, 2010, **312**, 2107.
64 A. Arakaki, H. Nakazawa, M. Nemoto, T. Mori and T. Matsunaga, *J. R. Soc. Interface*, 2008, **5**, 977.
65 K. Katagiri, Y. Imai, K. Koumoto, T. Kaiden, K. Kono and S. Aoshima, *Small*, 2011, **7**, 1683.
66 A. Kanazawa, S. Kanaoka, N. Yagita, Y. Oaki, H. Imai, M. Oda, A. Arakaki, T. Matsunaga and S. Aoshima, *Chem. Commun.*, 2012, **48**, 10904.
67 T. Osaka, T. Matsunaga, T. Nakanishi, A. Arakaki, D. Niwa and H. Iida, *Anal. Bioanal. Chem.*, 2006, **384**, 593.
68 R. P. Blakemore, *Nature*, 1975, **190**, 377.
69 T. Matsunaga, Y. Okamura, Y. Fukuda, A. T. Wahyudi, Y. Murase and H. Takeyama, *DNA Res.*, 2005, **12**, 157.
70 H. Nakazawa, A. Arakaki, S. Narita-Yamada, I. Yashiro, K. Jinno, N. Aoki, A. Tsuruyama, Y. Okamura, S. Tanikawa, N. Fujita, H. Takeyama and T. Matsunaga, *Genome Res.*, 2009, **19**, 1801.
71 T. Suzuki, Y. Okamura, R. J. Calugay, H. Takeyama and T. Matsunaga, *J. Bacteriol.*, 2006, **188**, 2275.
72 M. Tanaka, Y. Okamura, A. Arakaki, T. Tanaka, H. Takeyama and T. Matsunaga, *Proteomics*, 2006, **6**, 5234.
73 A. Komeili, *FEMS Microbiol. Rev.*, 2012, **36**, 232.
74 D. Schüler, *FEMS Microbiol. Rev.*, 2008, **32**, 654.

75 M. Tanaka, A. Arakaki and T. Matsunaga, *Mol. Microbiol.*, 2010, **76**, 480.
76 A. Komeili, H. Vali, T. J. Beveridge and D. K. Newman, *Proc. Natl. Acad. Sci. U. S. A.*, 2004, **101**, 3839.
77 N. Zeytuni, E. Ozyamak, K. Ben-Harush, G. Davidov, M. Levin, Y. Gat, T. Moyal, A. Brik, A. Komeili and R. Zarivach, *Proc. Natl. Acad. Sci. U. S. A.*, 2011, **108**, E480.
78 Y. Okamura, H. Takeyama and T. Matsunaga, *J. Biol. Chem.*, 2001, **276**, 48183.
79 C. Nakamura, J. G. Burgess, K. Sode and T. Matsunaga, *J. Biol. Chem.*, 1995, **270**, 28392.
80 D. Murat, A. Quinlan, H. Vali and A. Komeili, *Proc. Natl. Acad. Sci. U. S. A.*, 2010, **107**, 5593.
81 R. Uebe, K. Junge, V. Henn, G. Poxleitner, E. Katzmann, J. M. Plitzko, R. Zarivach, T. Kasama, G. Wanner, M. Posfai, L. Bottger, B. Matzanke and D. Schüler, *Mol. Microbiol.*, 2011, **82**, 818.
82 M. I. Siponen, P. Legrand, M. Widdra, S. R. Jones, W. J. Zhang, M. C. Chang, D. Faivre, P. Arnoux and D. Pignol, *Nature*, 2013, **502**, 681.
83 A. Komeili, Z. Li, D. K. Newman and G. J. Jensen, *Science*, 2006, **311**, 242.
84 A. Scheffel, M. Gruska, D. Faivre, A. Linaroudis, J. M. Plitzko and D. Schüler, *Nature*, 2006, **440**, 110.
85 Y. Amemiya, A. Arakaki, S. S. Staniland, T. Tanaka and T. Matsunaga, *Biomaterials*, 2007, **28**, 5381.
86 L. Wang, T. Prozorov, P. E. Palo, X. Liu, D. Vaknin, R. Prozorov, S. Mallapragada and M. Nilsen-Hamilton, *Biomacromolecules*, 2012, **13**, 98.
87 M. Tanaka, E. Mazuyama, A. Arakaki and T. Matsunaga, *J. Biol. Chem.*, 2011, **286**, 6386.
88 A. Arakaki, A. Yamagishi, A. Fukuyo, M. Tanaka and T. Matsunaga, *Mol. Microbiol.*, 2014, **93**, 554.
89 F. Vereda, J. de Vicente and R. Hidalgo-Alvarez, *J. Colloid Interface Sci.*, 2013, **392**, 50.
90 A. Arakaki, F. Masuda, Y. Amemiya, T. Tanaka and T. Matsunaga, *J. Colloid Interface Sci.*, 2010, **343**, 65.
91 T. Prozorov, P. Palo, L. Wang, M. Nilsen-Hamilton, D. Jones, D. Orr, S. K. Mallapragada, B. Narasimhan, P. C. Canfield and R. Prozorov, *ACS Nano*, 2007, **1**, 228.
92 J. M. Galloway, A. Arakaki, F. Masuda, T. Tanaka, T. Matsunaga and S. S. Staniland, *J. Mater. Chem.*, 2011, **21**, 15244.
93 A. Arakaki, F. Masuda and T. Matsunaga, *Mater. Res. Soc. Symp. Proc.*, 2009, **1187**, KK03.
94 J. Galloway, J. Bramble, A. Rawlings, G. Burnell, S. Evans and S. Staniland, *Small*, 2012, **8**, 204.
95 J. H. Cartwright, A. G. Checa, J. D. Gale, D. Gebauer and C. I. Sainz-Diaz, *Angew. Chem., Int. Ed.*, 2012, **51**, 11960.
96 J. Ihli, W. C. Wong, E. H. Noel, Y.-Y. Kim, A. N. Kulak, H. K. Christenson, M. J. Duer and F. C. Meldrum, *Nat. Commun.*, 2014, **5**, 3169, DOI: 10.1038/ncomms4169.
97 E. H. Noel, Y.-Y. Kim, J. M. Charnock and F. C. Meldrum, *CrystEngComm*, 2013, **15**, 697.
98 S.-F. Chen, H. Coelfen, M. Antonietti and S.-H. Yu, *Chem. Commun.*, 2013, **49**, 9564.
99 L. B. Gower, *Chem. Rev.*, 2008, **108**, 4551.
100 T. Kato, T. Sakamoto and T. Nishimura, *MRS Bull.*, 2010, **35**, 127.
101 F. C. Meldrum, *Int. Mater. Rev.*, 2003, **48**, 187.
102 N. A. Sommerdijk and G. de With, *Chem. Rev.*, 2008, **108**, 4499.
103 A. Sugawara-Narutaki, *Polym. J.*, 2013, **45**, 269.
104 T. Kato, T. Suzuki and T. Irie, *Chem. Lett.*, 2000, **29**, 186.
105 T. Kato, *Adv. Mater.*, 2000, **12**, 1543.
106 T. Kato, T. Suzuki, T. Amamiya, T. Irie, M. Komiyama and H. Yui, *Supramol. Sci.*, 1998, **5**, 411.
107 A. Sugawara and T. Kato, *Chem. Commun.*, 2000, 487.
108 A. Sugawara and T. Kato, *Compos. Interfaces*, 2004, **11**, 287.
109 N. Hosoda and T. Kato, *Chem. Mater.*, 2001, **13**, 688.
110 N. Hosoda, A. Sugawara and T. Kato, *Macromolecules*, 2003, **36**, 6449.
111 A. Sugawara, T. Ishii and T. Kato, *Angew. Chem., Int. Ed.*, 2003, **42**, 5299.
112 F. Zhu, T. Nishimura, H. Eimura and T. Kato, *CrystEngComm*, 2014, **16**, 1496–1501.
113 A. Sugawara, T. Nishimura, Y. Yamamoto, H. Inoue, H. Nagasawa and T. Kato, *Angew. Chem., Int. Ed.*, 2006, **45**, 2876.
114 J. E. Rebers and L. M. Riddiford, *J. Mol. Biol.*, 1988, **203**, 411.
115 A. Hecker, O. Testeniere, F. Marin and G. Luquet, *FEBS Lett.*, 2003, **535**, 49.
116 H. Inoue, T. Ohira and H. Nagasawa, *Peptides*, 2007, **28**, 566.
117 Y. Yamamoto, T. Nishimura, A. Sugawara, H. Inoue, H. Nagasawa and T. Kato, *Cryst. Growth Des.*, 2008, **8**, 4062.
118 H. Kumagai, R. Matsunaga, T. Nishimura, Y. Yamamoto, S. Kajiyama, Y. Oaki, K. Akaiwa, H. Inoue, H. Nagasawa, K. Tsumoto and T. Kato, *Faraday Discuss.*, 2012, **159**, 483.
119 J. Aizenberg, A. J. Black and G. M. Whitesides, *J. Am. Chem. Soc.*, 1999, **121**, 4500.
120 S. Tugulu, M. Harms, M. Fricke, D. Volkmer and H. A. Klok, *Angew. Chem., Int. Ed.*, 2006, **45**, 7458.
121 S. Kumar, T. Ito, Y. Yanagihara, Y. Oaki, T. Nishimura and T. Kato, *CrystEngComm*, 2010, **12**, 2021.
122 Y. Han, T. Nishimura and T. Kato, *CrystEngComm*, 2014, **16**, 3540.
123 Y. Han, T. Nishimura and T. Kato, *Polym. J.*, 2014, **46**, 499.
124 Y.-Y. Kim, A. S. Schenk, D. Walsh, A. N. Kulak, O. Cespedesc and F. C. Meldrum, *Nanoscale*, 2014, **6**, 852.
125 S.-S. Wang, A. Picker, H. Coelfen and A.-W. Xu, *Angew. Chem., Int. Ed.*, 2013, **52**, 6317.
126 Y.-Y. Kim, A. S. Schenk, J. Ihli, A. N. Kulak, N. B. J. Hetherington, C. C. Tang, W. W. Schmahl, E. Griesshaber, G. Hyett and F. C. Meldrum, *Nat. Commun.*, 2014, **5**, 4341, DOI: 10.1038/ncomms5341.
127 Y. Jiang, H. Gong, M. Grzywa, D. Volkmer, L. Gower and H. Coelfen, *Adv. Funct. Mater.*, 2013, **23**, 1547.
128 H. Tomono, H. Nada, F. Zhu, T. Sakamoto, T. Nishimura and T. Kato, *J. Phys. Chem. B*, 2013, **117**, 14849.

129 F. Zhu, T. Nishimura, T. Sakamoto, H. Tomono, H. Nada, Y. Okumura, H. Kikuchi and T. Kato, *Chem. – Asian J.*, 2013, **8**, 3002.
130 T. Nishimura, T. Ito, Y. Yamamoto, M. Yoshio and T. Kato, *Angew. Chem., Int. Ed.*, 2008, **47**, 2800.
131 H. Coelfen and M. Antonietti, *Angew. Chem., Int. Ed.*, 2005, **44**, 5576.
132 Y. Bouligand, *Tissue Cell*, 1972, **4**, 189.
133 J. E. Lydon, *Liq. Cryst. Today*, 2004, **13**, 1.
134 Y. Yamamoto, T. Nishimura, T. Saito and T. Kato, *Polym. J.*, 2010, **42**, 583.
135 T. Saito, Y. Oaki, T. Nishimura, A. Isogai and T. Kato, *Mater. Horiz.*, 2014, **1**, 321.
136 T. Sakamoto, A. Oichi, T. Nishimura, A. Sugawara and T. Kato, *Polym. J.*, 2009, **41**, 522.
137 T. Sakamoto, A. Oichi, Y. Oaki, T. Nishimura, A. Sugawara and T. Kato, *Cryst. Growth Des.*, 2009, **9**, 622.
138 T. Sakamoto, Y. Nishimura, T. Nishimura and T. Kato, *Angew. Chem., Int. Ed.*, 2011, **50**, 5856.
139 S. Kajiyama, T. Nishimura, T. Sakamoto and T. Kato, *Small*, 2014, **10**, 1634.
140 X. Wu and S. Wang, *Adv. Healthcare Mater.*, 2013, **2**, 326.